Value of ^{68}Ga-PSMA HBED-CC PET for the Assessment of Lymph Node Metastases in Prostate Cancer Patients with Biochemical Recurrence: Comparison with Histopathology After Salvage Lymphadenectomy

Isabel Rauscher*[1], Tobias Maurer*[2], Ambros J. Beer[3], Frank-Philipp Graner[1], Bernhard Haller[4], Gregor Weirich[5], Alan Doherty[6], Jürgen E. Gschwend[2], Markus Schwaiger[1], and Matthias Eiber[1]

[1]Department of Nuclear Medicine, Klinikum Rechts der Isar, Technische Universität München, Munich, Germany; [2]Department of Urology, Klinikum Rechts der Isar, Technische Universität München, Munich, Germany; [3]Department of Nuclear Medicine, University Hospital Ulm, Ulm, Germany; [4]Institute of Medical Statistics and Epidemiology, Klinikum Rechts der Isar, Technische Universität München, Munich, Germany; [5]Department of Pathology, Klinikum Rechts der Isar, Technische Universität München, Munich, Germany; and [6]Queen Elizabeth Hospital, University Hospitals Birmingham NHS Foundation Trust, Edgbaston, Birmingham, United Kingdom

The purpose of this study was to evaluate the accuracy of Glu-NH-CO-NH-Lys-(Ahx)-[^{68}Ga(HBED-CC)] PET compared with morphologic imaging for the assessment of lymph node metastases (LNM) in patients with recurrent prostate cancer. **Methods:** Forty-eight patients (median age, 71 y; interquartile range, 66–74 y) with biochemical recurrence (median prostate-specific antigen level, 1.31 ng/mL; interquartile range, 0.75–2.55 ng/mL) who underwent ^{68}Ga–prostate-specific membrane antigen (PSMA) HBED-CC PET/CT or PET/MR and salvage lymphadenectomy were retrospectively included. Institutional review board approval and written informed consent were obtained from all patients for the purpose of anonymized evaluation and publication of their data. Standardized predefined lymph node (LN) template fields ($n = 10$) were evaluated in ^{68}Ga-PSMA HBED-CC PET and morphologic imaging for the presence of LNM using a 5-point-scale. Additionally, SUV$_{mean/max}$ and size of suspicious lesions were determined. Specificity of ^{68}Ga-PSMA HBED-CC PET imaging for PET-positive LNs was defined by comparison to histopathology. The diagnostic accuracy of ^{68}Ga-PSMA HBED-CC PET compared with morphologic imaging alone was assessed, and areas under the receiver-operating-characteristic curves are presented. **Results:** LNM were found histologically in 68 of 179 resected anatomic LN fields (38.0%). The specificity of ^{68}Ga-PSMA HBED-CC PET and morphologic imaging was 97.3% and 99.1%, respectively. However, ^{68}Ga-PSMA HBED-CC PET detected LNM in 53 of 68 histopathologically proven metastatic LN fields (77.9%) whereas morphologic imaging was positive in only 18 of 67 (26.9%). ^{68}Ga-PSMA HBED-CC PET imaging performed significantly superior to morphologic imaging for detection of LNM (difference in the areas under the receiver-operating-characteristic curves, 0.139; 95% confidence interval, 0.063–0.214; $P < 0.001$). In ^{68}Ga-PSMA HBED-CC PET, the mean size of PET-positive LN measured by CT or MRI was 8.3 ± 4.3 mm (range, 4–25 mm), and LNs, which were suspicious only in CT or MRI, presented with a mean size of 13.0 ± 4.9 mm (range, 8–25 mm). **Conclusion:** ^{68}Ga-PSMA HBED-CC PET imaging is a promising method for early detection of LNM in patients with biochemical recurrent prostate cancer. It is more accurate than morphologic imaging and thus might represent a valuable tool for guiding salvage lymphadenectomy.

Key Words: positron emission tomography; magnetic resonance imaging; computed tomography; hybrid imaging; ^{68}Ga-PSMA HBED-CC; prostate cancer; salvage lymphadenectomy

Biochemical recurrence after definitive treatment of prostate cancer (PC) occurs in up to 50% of cases (*1–3*). Serum prostate-specific antigen (PSA) testing is routinely used to detect PC recurrence. However, PSA testing does not allow for distinguishing between local, regional, or distant recurrence. Because the use of lesion-targeted management options including salvage lymphadenectomy or targeted irradiation therapy in patients with minimal or localized metastatic tumor load are increasingly favored, a correct identification of recurrent disease is essential for further treatment planning (*4,5*).

At present, accuracy of currently widely available imaging modalities is suboptimal in identifying lymph node metastases (LNM) in patients with recurrent PC. Promising results have been published for the use of ultra-small superparamagnetic iron oxide particles (*6*). However, so far they are not routinely available. The limited role of conventional morphologic imaging techniques such as CT or MRI in the detection of local recurrence and LNM in patients with recurrent disease is well known, with sensitivities reaching only 13%–40% (*7,8*). Further, the performance of CT and MR is not significantly different from what could be demonstrated in a large meta-analysis including 24 studies. Here, the pooled sensitivity was 42% and 39% and the pooled specificity was 82% and 82% for CT and MR, respectively (*7*).

These limitations might be overcome by molecular imaging techniques (*9*). For example, ^{11}C-choline PET/CT can detect LNM

in recurrent PC sensitively, however, it is not able to detect small-volume lesions (10). Furthermore, the detection rate of ^{11}C-choline PET/CT at PSA levels below 1 ng/mL is limited, with only 36% of positive findings, and thus not regarded as appropriate for the detection of early recurrent disease (11). Specificity, on the other hand, is regarded as satisfactory, with a pooled value of 89% being reported in a recent meta-analysis summarizing 29 studies evaluating ^{11}C-choline PET (12).

Recently, a ^{68}Ga-labeled ligand of the prostate-specific membrane antigen (PSMA) Glu-NH-CO-NH-Lys-(Ahx)-[[68]Ga(HBED-CC)], often termed ^{68}Ga-PSMA HBED-CC or ^{68}Ga-PSMA-11, has been introduced in PET imaging for PC, with highly promising results (13–15). Because of increased expression of PSMA in PC and its metastases, ^{68}Ga-PSMA HBED-CC PET was reported to exhibit a favorable lesion-to-background ratio with high detection rates (16). Further, recent studies evaluating ^{68}Ga-PSMA HBED-CC PET showed substantially higher detection rates in patients with recurrent PC than reported for other imaging modalities, especially at low PSA values (<0.5 ng/mL) (17,18). However, in both studies histopathology as a gold standard was available only in a minority of cases. One recent large study performing preoperative lymph node (LN) staging using ^{68}Ga-PSMA HBED-CC PET in primary PC, however, showed a high accuracy of ^{68}Ga-PSMA HBED-CC PET, with a superb specificity of 99.1% (19).

Thus, the aim of our study was to evaluate the accuracy of ^{68}Ga-PSMA HBED-CC PET compared with morphologic imaging for the detection of LNM in patients with recurrent PC after primary treatment validated by histopathology.

MATERIALS AND METHODS

Patient Population

All patients (November 2012 to June 2015) with biochemical recurrence (PSA > 0.2 ng/mL) who underwent salvage lymphadenectomy after ^{68}Ga-PSMA HBED-CC PET/CT or PET/MR were extracted from the institution's database. Thirteen patients in the present evaluation were partially analyzed in a previous study (18). All patients were treated initially for localized PC by radical prostatectomy and pelvic lymphadenectomy ($n = 45$; 93.8%) or radiation therapy ($n = 3$; 6.2%) with curative intent. None of the patients had received androgen-deprivation therapy within the last 6 mo before the examination.

All patients had undergone open salvage lymphadenectomy, with the extent of lymphadenectomy being dependent on preoperative imaging results, patients' risk factors, and intraoperative findings (in some patients no tissue was left after previous lymphadenectomy or extensive fibrotic changes precluded resection of further fields not suspicious on preoperative imaging). During lymphadenectomy, tissue from each resected LN field was sent separately for histologic evaluation. Surgical specimens were processed according to standard pathology protocols.

The retrospective study was approved by the Ethics Committee of the Technical University Munich (permit 5665/13), and written informed consent was obtained from all patients for the purpose of anonymized evaluation and publication of their data. All reported investigations were conducted in accordance with the Helsinki Declaration and with national regulations.

[68]Ga-Labeled HBED-CC PET Application and Imaging

[68]Ga-labeled HBED-CC was produced as previously described (20). The ^{68}Ga-PSMA HBED-CC-ligand complex solution (1.8–2.2 MBq per kg of body weight) was applied intravenously (mean, 154 MBq;

interquartile range [IQR], 133–179 MBq), and PET acquisition was started at a mean time of 57 min (IQR, 49–63 min) after tracer injection. Thirty-one patients underwent ^{68}Ga-PSMA HBED-CC PET/CT on a Biograph mCT scanner (Siemens Medical Solutions), and 17 patients underwent ^{68}Ga-PSMA HBED-CC PET/MR on a fully integrated whole-body hybrid PET/MR system (Biograph mMR; Siemens Healthcare). PET/CT included a diagnostic CT (240 mAS, 120 kV, 5-mm slice thickness) in the portal venous phase (80 s after injection of the intravenous contrast agent). For the assessment of the presence of LNM in PET/MR, an axial T2 turbo spin echo sequence of the pelvis and an axial T2 half Fourier acquisition single-shot turbo spin echo of the whole body was used. Details on the complete protocol in PET/MR and PET/CT have been described previously (18,21). For PET/CT, the emission time was 4 min per bed position, whereas for PET/MR the emission time for the trunk was 5 min per bed position. All PET images were acquired in 3-dimensional mode and reconstructed by an attenuation-weighted ordered-subsets expectation maximization algorithm (4 iterations, 8 subsets) followed by a postreconstruction smoothing gaussian filter (5 mm in full width at half maximum).

Image Analysis and Quantitative Assessment

The entire rating procedure was performed using a dedicated workstation and software (Syngo MMWP and Syngo TrueD; Siemens Medical Solutions). First, images were analyzed by 1 double-trained board-certified radiologist and nuclear medicine physician with 9 y of training in oncologic imaging masked to the patient history and the extent of performed lymphadenectomy. Thus, in every patient in total and in a standardized way the following 10 anatomic fields were evaluated: right/left common iliac vessel, right/left internal iliac vessel, right/left external iliac vessel, right/left obturator fossa, presacral and other regions, for example, paraaortic LNs.

In PET, every anatomic field was rated on a 5-point-scale using the following criteria: 1, tumor manifestation (intense, focal ^{68}Ga-PSMA HBED-CC uptake higher than liver); 2, probably tumor manifestation (^{68}Ga-PSMA HBED-CC uptake clearly higher than background in vessels but not higher than liver); 3, equivocal (^{68}Ga-PSMA HBED-CC faint uptake between background in muscle and vessels); 4, probably benign (^{68}Ga-PSMA HBED-CC uptake as faint as background, e.g., equally to adjacent muscle); and 5, benign (no ^{68}Ga-PSMA HBED-CC uptake). Hereby, anatomic images were used only for anatomic allocation of a suspicious focal increased uptake to the corresponding LN field.

In a second step, with a time interval of at least 4 wk, the diagnostic CT or MR dataset was analyzed for LNM using morphologic criteria (size, short axis; shape; and regional grouping) (7). Each anatomic field was rated on a 5-point-scale using the following criteria: 1, tumor manifestation (short-axis diameter > 10 mm); 2, probably tumor manifestation (short-axis diameter, 8–10 mm; round configuration; or regional grouping); 3, equivocal (short-axis diameter, 8–10 mm; oval configuration; and no regional grouping); 4, probably benign (short-axis diameter < 8 mm); and 5, benign (short-axis diameter < 5 mm).

For quantitative analysis, a resident with 4 y of experience in oncologic imaging noted the highest SUV in each suspicious LN field. If multiple LNs were suspicious in 1 anatomic field, only the one with the highest uptake was analyzed. To calculate SUVs, an isocontour volume of interest including all voxels above 50% of the maximum was created, covering the whole lesion volume. Within all volumes of interest, mean and maximum SUVs were measured. In addition, size (maximum short diameter in mm) of PET-positive lesions and suspicious LNs in the morphologic MR or CT dataset were measured. If multiple LNs were suspicious in 1 anatomic field, only the largest one was measured.

Statistical Analysis

All statistical analyses were performed using MedCalc software (version 13.2.0, 2014; MedCalc). Histopathologic findings of resected LNs were compared with the results of morphologic imaging (MR or CT) alone and ^{68}Ga-PSMA HBED-CC PET imaging in a field-based manner. This approach was chosen, because exact tracking of a single LN is impossible without further guidance, for example, by radiolabeled colloid or PSMA ligands (especially in the case of normal-sized LNs because of disorientation during resection and histologic evaluation).

Overall diagnostic accuracy using field-based and patient-based data was assessed conducting receiver-operating characteristics (ROC) analyses. For both modalities (^{68}Ga-PSMA HBED-CC PET, morphologic imaging), ROC curves were calculated, and the areas under the ROC curves (AUCs) are presented. For estimation of 95% confidence intervals (CIs) and for comparison of the modalities, the nonparametric method proposed by Obuchowski was used to account for the correlation of multiple observations within the same patients ([22]).

After dichotomization of the qualitative assessments (≤ 2, positive test; > 2, negative test), sensitivities, specificities, and accuracies were estimated for both modalities. For field-based analysis, CIs were derived from logistic generalized estimating equation models ([23]). For estimation of sensitivities and corresponding CIs, an intercept-only logistic generalized estimating equation model was fitted to the data. The result of the dichotomized test was used as a dependent variable, and only patients with a positive histopathologic result were considered ([24]). To derive estimates for the specificities, a variable indicating whether a negative test result was observed was used as a dependent variable, and only patients with a negative histopathologic result were included. Accuracy was estimated in an intercept-only model with a dependent variable that indicated whether the test result and the result of the histopathologic assessment agreed. For all generalized estimating equation models, an independent correlation structure was assumed.

RESULTS

Patient Characteristics

Forty-eight patients were included in the analysis (median age, 71 y; IQR, 66–74 y). Median time between imaging and salvage lymphadenectomy was 47 d (IQR, 28–67 d). In 4 of those 48 patients, salvage lymphadenectomy was performed in an external hospital. However, in all patients detailed surgical and histologic reports were available. A median of 3 LN fields (range, 1–9) per patient were resected during salvage lymphadenectomy. The median primary Gleason score was 7 (IQR, 7–9), and median PSA level at time of PET imaging was 1.31 ng/mL (IQR, 0.75–2.55 ng/mL).

Histopathologic Results

In total, LNM were found in 68 of 179 resected anatomic LN fields (38.0%) after histopathologic workup. The metastatic LNs were located in the following regions: right common iliac vessel ($n = 6$), left common iliac vessel ($n = 7$), right internal iliac vessel ($n = 4$), left internal iliac vessel ($n = 9$), right external iliac vessel ($n = 6$), left external iliac vessel ($n = 9$), right obturator fossa ($n = 7$), left obturator fossa ($n = 3$), presacral ($n = 9$) or other regions, for example, paraaortic ($n = 8$). Details on the operated LN fields and the percentage of LNM in each LN field are shown in Table 1.

Imaging Findings

On a field-based analysis, specificity of ^{68}Ga-PSMA HBED-CC PET was 97.3% (95% CI, 91.9%–99.1%) and 99.1% (95% CI, 93.9%–99.9%) for morphologic imaging, respectively. However,

^{68}Ga-PSMA HBED-CC PET detected LNM in 53 of 68 histopathologically proven metastatic LN fields (77.9%; 95% CI, 65.1%–87.0%), whereas morphologic imaging was positive in only 18 of 67 (26.9%; 95% CI, 16.2%–41.1%). The positive predictive value was 94.6% for PET and 94.7% for morphologic imaging. Diagnostic accuracy of ^{68}Ga-PSMA HBED-CC PET imaging was 89.9% (95% CI, 82.5%–94.4%) and for morphologic imaging 71.9% (95% CI, 61.8%–80.2%), respectively (Table 2).

In detail, 111 fields were free of tumor invasion after histopathologic evaluation, with 108 of them being correctly identified as negative with PET and 110 of them being correctly identified as negative with morphologic imaging. One metastatic LN field could not be evaluated in CT because of clip material located in the pelvis. Three fields in 3 patients were classified as suspicious in PET with no correlation in histopathology (false-positive), whereas in morphologic imaging 1 field was judged false-positive. Fifteen fields (in 9/48 patients) were false-negative in PET, whereas in morphologic imaging 49 fields revealed a false-negative finding.

AUC for ^{68}Ga-PSMA HBED-CC PET imaging and morphologic imaging was 0.878 (95% CI, 0.819–0.937) and 0.738 (95% CI, 0.660–0.816), respectively (Fig. 1). ^{68}Ga-PSMA HBED-CC PET imaging performed significantly better than morphologic imaging on a field-based analysis for detection of LNM (difference in AUCs, 0.139; 95% CI, 0.063–0.214; $P < 0.001$).

On a patient-based analysis, sensitivity, specificity, and accuracy of ^{68}Ga-PSMA HBED-CC PET and morphologic imaging were 100%, 50%, and 93.8% versus 34.1%, 83.3%, and 40.4%, respectively (Table 3). The AUC for ^{68}Ga-PSMA HBED-CC PET and morphologic imaging was 0.732 (95% CI, 0.583–0.850) and 0.665 (95% CI, 0.512–0.796), respectively. There was no significant difference between ^{68}Ga-PSMA HBED-CC PET and morphologic imaging for the detection of LNM on a patient-based analysis (difference in AUCs, 0.0671; 95% CI, −0.241 to 0.376; $P = 0.6701$).

In ^{68}Ga-PSMA HBED-CC PET, the mean SUV_{mean} of suspicious LN was 9.0 ± 7.5 (range, 1.8–36.0), and mean SUV_{max} was 12.7 ± 10.8 (range, 2.4–51.0). Corresponding mean lesion size of ^{68}Ga-PSMA HBED-CC PET–suspicious LN in CT or MRI was 8.3 ± 4.3 mm (range, 4–25 mm). The mean size of LN suspicious only in morphologic imaging was 13.0 ± 4.9 mm (range, 8–25 mm). Histopathologic workup of false-negative LN fields in ^{68}Ga-PSMA HBED-CC PET revealed a mean lesion size of 4.7 ± 3.4 mm (range, 0.5–11 mm). Representative examples of correctly classified LNM by ^{68}Ga-PSMA HBED-CC PET/CT and representative false-negative findings are shown in Figures 2 and 3.

DISCUSSION

Several first studies have demonstrated the high clinical value of ^{68}Ga-PSMA HBED-CC PET/CT in patients with recurrent PC after primary treatment ([17,18,25,26]). Besides reporting first on the superior performance of ^{68}Ga-PSMA HBED-CC PET/CT mainly in recurrent PC, Afshar-Oromieh et al. also demonstrated a high specificity of ^{68}Ga-PSMA HBED-CC PET in a subgroup of patients with histologic verification ([17]). In addition, so far only 2 further studies reported on the use of ^{68}Ga-PSMA HBED-CC PET for LN restaging with histologic evaluation of all patients ([25,26]). However, both studies encompass not only patients scheduled for restaging after biochemical failure but also patients undergoing primary radical prostatectomy including lymphadenectomy. Thus, to the best of our knowledge, this is the first report presenting data on the performance of ^{68}Ga-PSMA HBED-CC PET in a homogeneous

TABLE 1
Total Number and Location of Resected LN Fields and Histopathologically Proven LNM

LN fields	No. of resected fields	No. of histopathologically proven LNM	% of histopathologically proven LNM
Level 1 right common iliac vessel	18	6	33.3
Level 2 left common iliac vessel	22	7	31.8
Level 3 right internal iliac vessel	16	4	25
Level 4 left internal iliac vessel	20	9	45
Level 5 right external iliac vessel	17	6	35.3
Level 6 left external iliac vessel	19	9	47.4
Level 7 right obturator fossa	18	7	38.9
Level 8 left obturator fossa	18	3	16.7
Level 9 presacral	13	9	69.2
Level 10 others	18	8	44.4

patient collective with biochemical recurrence after primary definite treatment using histopathology as a standard of reference for all cases.

Our study demonstrates that ^{68}Ga-PSMA HBED-CC PET is a highly accurate tool in detecting LNM in recurrent PC, with a sensitivity, specificity, and accuracy of 77.9%, 97.3%, and 89.9%, respectively. Morphologic imaging was considerably less sensitive (26.9%) and accurate (71.9%), with an equal performance regarding specificity (99.1%). The latter is most likely explained by the use of strict criteria for morphologic assessment of LNM with a short-axis diameter of greater than 10 mm for rating 1 (tumor manifestation) and a short diameter of 8–10 mm and additional round configuration or regional grouping for rating 2 (probably tumor manifestation).

The recent study by Herlemann et al. evaluating ^{68}Ga-PSMA HBED-CC PET in a mixed group of primary PC ($n = 20$) and recurrent PC ($n = 14$) showed a sensitivity of 84% and specificity of 82% for PET for all patients as well as a clear superiority in diagnostic accuracy of PET versus CT, with 77% versus 65% for the subgroup of patients with salvage lymphadenectomy (28).

Taken together, both the data presented by this work and that of Herlemann et al. strengthen the value of ^{68}Ga-PSMA HBED-CC PET for preoperative staging. The other study by Hijazi et al. investigated ^{68}Ga-PSMA HBED-CC PET/CT also in a mixed group of patients with biochemical recurrence and primary PC, judging 8 different LN fields in imaging (25). The authors reported a high specificity of 99% similar to our data. However, they found a considerably higher sensitivity of 94% than found in our data stating that only 78% of histopathologically positive LN fields were detected. As in the work by Hijazi et al., extended LN dissection was available in only 17 of 35 patients, thus the true extent of LNM could have be underestimated.

In addition, the presented data are well comparable to a large series of patients with intermediate- to high-risk PC in the setting of primary LN staging using ^{68}Ga-PSMA HBED-CC PET. Maurer et al. reported a sensitivity, specificity, and accuracy for ^{68}Ga-PSMA HBED-CC PET of 78.2%, 99.1%, and 95.7%, respectively (19). Further, ^{68}Ga-PSMA HBED-CC PET performed significantly superior to morphologic imaging alone (difference in AUCs, 0.174; 95% CI, 0.114–0.233; $P < 0.001$), which is also

TABLE 2
Results and Diagnostic Values for Detection of LNM on Field-Based Analysis

Results	Histology: LNM		Diagnostic accuracy
	Positive	Negative	
^{68}Ga-PSMA HBED-CC PET rating			
Positive	53	3	PPV, 94.6%
Negative	15	108	NPV, 87.8%
Total	68	111	179
	Sensitivity, 77.9%	Specificity, 97.3%	Accuracy, 89.9%
Morphologic rating (CT/MR)			
Positive	18	1	PPV, 94.7%
Negative	49	110	NPV, 69.2%
Total	67	111	178
	Sensitivity, 26.9%	Specificity, 99.1%	Accuracy, 71.9%

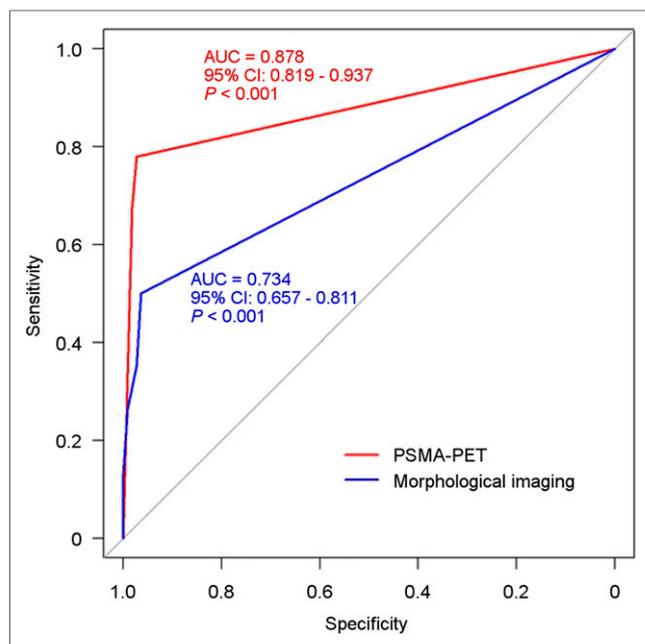PPV = positive predictive value; NPV = negative predictive value.

FIGURE 1. ROC curves for ^{68}Ga-PSMA HBED-CC PET imaging (red) and morphologic imaging (CT/MR) (blue) for detection of LNM on a field-based analysis (*P* values: comparison to AUC = 0.5).

similar to the results of this study (difference in AUCs, 0.139; 95% CI, 0.063–0.214; *P* < 0.001).

When our results are compared with studies of other PET agents, Rinnab et al., evaluating ^{11}C-choline PET/CT in patients with recurrent PC at a PSA level of less than 2.5 ng/mL, reported a sensitivity of 91% and specificity of 50% in a patient-based analysis (*27*). These values are comparable to the results for ^{68}Ga-PSMA HBED-CC on a patient-based level in our study. However, the median PSA level of patients examined by Rinnab et al. was 2.42 ng/mL, compared with 1.31 ng/mL in our study. In addition, caution is warranted because the high sensitivity in both studies when reporting data on a patient basis is strongly influenced by

imaging-derived preselection. The lack of a statistical significance for our data when presented on a patient basis comparing ^{68}Ga-PSMA HBED-CC PET versus morphologic imaging is most likely due to the considerably smaller sample size as opposed to a field-based approach.

Using a site- or lesion-based analysis, Scattoni et al. reported a sensitivity, specificity, positive predictive value, negative predictive value, and accuracy of 64%, 90%, 86%, 72%, and 77%, respectively, for ^{11}C-choline PET/CT (*10*). In contrast, another study identifying histologically confirmed LNM with ^{18}F-fluoroethylcholine PET/CT reported sensitivity, specificity, positive predictive value, and negative predictive value of 39.7%, 95.8%, 75.7%, and 83% in a site-based analysis, respectively (*28*). However, in this study only 3 different sites were evaluated separately, compared with up to 10 LN fields in our study collective. In total, compared with data from literature, our results suggest that PET using ^{68}Ga-PSMA HBED-CC seems to be more accurate than choline-based PET in the detection of LNM in recurrent PC. An improved tumor-to-background ratio facilitating the detection of suspicious lesions using ^{68}Ga-PSMA HBED-CC PET compared with ^{18}F-choline has already been shown (*16*). Indeed, we also found high SUVs in most histopathologically positive LN fields.

In our study, for ^{68}Ga-PSMA HBED-CC PET 15 false-negative fields in 9 patients were found. Interestingly, in 4 of 9 patients the false-negative fields were located adjacent to correctly classified metastatic LN fields. Therefore, 1 explanation might be problems with correct allocation of LN fields in PET and lymphadenectomy. Nevertheless, it is known that despite increased detection using ^{68}Ga-PSMA HBED-CC PET, microscopic lesions might still be missed (*19*). In addition, 3 false-positive LN fields in 3 patients were found with no histopathologic correlate. It is worth mentioning that 1 patient (PSA level 0.45 ng/mL) presented with an intense, focal ^{68}Ga-PSMA HBED-CC uptake in the left obturator fossa with follow-up ^{68}Ga-PSMA HBED-CC PET/MR 6 mo after operation later revealing an increasing focal uptake of ^{68}Ga-PSMA HBED-CC (Supplemental Fig. 1; supplemental materials are available at http://jnm.snmjournals.org). Therefore, it has to be assumed that during salvage lymphadenectomy this LN was not resected.

TABLE 3
Results and Diagnostic Values for Detection of LNM Using Patient-Based Analysis

Results	Histology: LNM		Diagnostic accuracy
	Positive	Negative	
^{68}Ga-PSMA HBED-CC PET rating			
Positive	42	3	PPV, 93.3%
Negative	0	3	NPV, 100%
Total	42	6	48
	Sensitivity, 100%	Specificity, 50%	Accuracy, 93.8%
Morphologic rating (CT/MR)			
Positive	14	1	PPV, 93.3%
Negative	27	5	NPV, 84.3%
Total	41	6	47
	Sensitivity, 34.1%	Specificity, 83.3%	Accuracy, 40.4%

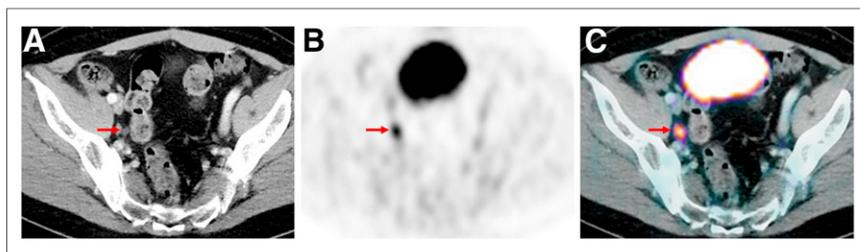PPV = positive predictive value; NPV = negative predictive value.

FIGURE 2. Example of a 55-y-old patient with biochemical recurrence after radical prostatectomy (Gleason score, 7; PSA level at PET examination, 0.77 ng/mL) and a correctly classified LNM by ^{68}Ga-PSMA HBED-CC PET imaging: a 6-mm LN is visible in right obturator fossa on CT imaging (A, arrow) that shows intense, focal and thus suspicious tracer uptake on ^{68}Ga-PSMA HBED-CC PET (B) and PET/CT fusion imaging (C). Salvage lymphadenectomy with histologic evaluation confirmed a single LNM.

From a clinical point of view, the high specificity provided by ^{68}Ga-PSMA HBED-CC highly predicts that a positive ^{68}Ga-PSMA HBED-CC PET scan will result in a histopathologically proven LNM in most patients or LN fields. In addition, compared with morphologic imaging alone, ^{68}Ga-PSMA HBED-CC PET can detect even small LNM with a lesion size below 10 mm (mean size of ^{68}Ga-PSMA HBED-CC–positive LN, 8.3 ± 4.3 vs. 13.0 ± 4.9 mm for suspicious LN on morphologic imaging). Because small lesions are difficult to detect intraoperatively, the intraoperative use of PSMA ligands during, for example, PSMA-radioguided surgery might become an important tool in guiding and improving resection of small prior ^{68}Ga-PSMA HBED-CC–positive LNs. Preliminary and encouraging experience on the use of ^{111}In PSMA imaging and therapy for radioguided surgery has recently been published (29).

There are several limitations to our study. First, despite extensive lymphadenectomy in 11 of 48 patients, in the remaining cases only LN fields adjacent to primary imaging-positive templates were resected. Thus, with regard to potential undetected distant lesions (e.g., LNM in distant templates not being positive in imaging), the positive predictive value is the only descriptive statistical value that is unaffected by this strong selection bias. Therefore, possible distant imaging-negative but histology-positive templates could have been missed, and therefore the sensitivity of the examined imaging technique might be underestimated. In addition, more robust data derived from prospective clinical trials are needed to validate the role of salvage lymphadenectomy guided by ^{68}Ga-PSMA HBED-CC PET for progression-free survival in this highly selected patient population (5). Because salvage lymphadenectomy was performed in an external hospital in 4 of 48 patients, only detailed surgical and histology reports were available in those cases. Because of a limited patient number in each subgroup, we cannot specifically compare the diagnostic value of ^{68}Ga-PSMA HBED-CC PET/MR with PET/CT. However, as indicated by several studies a similar performance for both PET of PET/MR and PET/CT and CT versus MR can be assumed. Regarding the diagnostic performance of PET, a recent study by Freitag et al. comparing ^{68}Ga-PSMA HBED-CC PET/MR with PET/CT in the evaluation of LNM and bone metastases of PC showed that both LNM and bone metastases are accurately and reliably depicted by ^{68}Ga-PSMA HBED-CC PET/MR, with low discordance compared with PET/CT including even PET-positive LNs of normal size (30). In their study, the correlation between SUVs of PET/MRI and PET/CT was linear in LNM and bone metastases. Further, there was no discordance in the number of suspicious LNs based on size criteria between CT and MRI. Additionally, a recent study by Spick et al. summarized data on more than 2,300 patients and concluded that ^{18}F-FDG PET/CT and PET/MRI perform equally well in different cancer types (31).

Furthermore, several studies (using ^{11}C-choline, ^{68}Ga-DOTATOC, or ^{18}F-FDG) have shown that PET datasets acquired by PET/MR and PET/CT are highly comparable (32–34). Regarding the diagnostic performance of CT and MR for detection of LNM, a meta-analysis by Hovels et al. showed that CT and MRI demonstrate an equally poor performance (7). In this study for CT, pooled sensitivity was 0.42 (95% CI, 0.26–0.56), and pooled specificity was 0.82 (95% CI, 0.8–0.83). For MRI, the pooled sensitivity was 0.39 (95% CI, 0.22–0.56), and pooled specificity was 0.82 (95% CI, 0.79–0.83). Further, in a recent work Giesel et al. showed in recurrent PC patients that ^{68}Ga-PSMA HBED-CC PET was able to detect LNM in two thirds of patients who would have been missed using conventional morphologic criteria (35). This result is in line with our observation that in ^{68}Ga-PSMA HBED-CC PET, the mean size of PET-positive LNs was considerably lower (8.3 ± 4.3 mm) than LNs suspicious only in CT or MRI (13.0 ± 4.9 mm).

Finally, for PET/MR it is known that highly specific tracers such as DOTA conjugates and PSMA ligands can cause a reduced signal
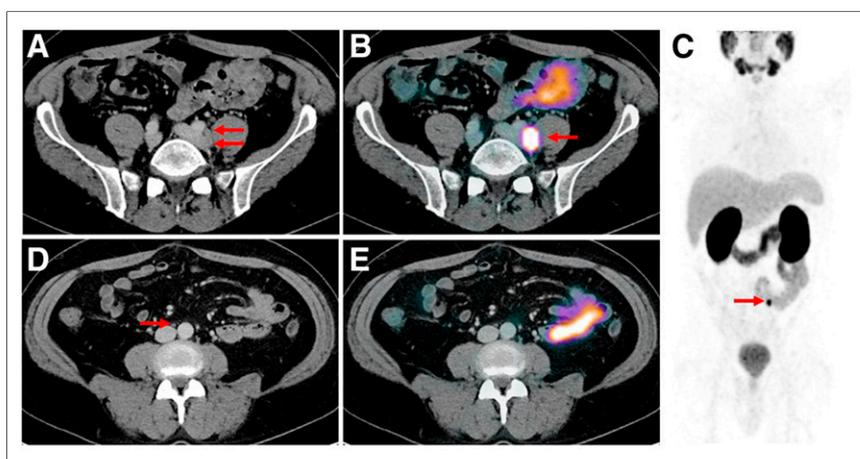

FIGURE 3. ^{68}Ga-PSMA HBED-CC PET imaging of a 55-y-old patient with recurrent PC (Gleason score, 8; PSA level at PET examination, 5.1 ng/mL). Patient presented with 2 correctly classified LNM (5 and 6 mm) behind left common iliac artery with intense, focal uptake on ^{68}Ga-PSMA HBED-CC PET/CT fusion (B, arrow) and on maximum-intensity-projection images (C, arrow). However, paraaortal/interaortocaval LN field was negative on ^{68}Ga-PSMA HBED-CC PET, showing no increased uptake either on maximum-intensity-projection images (C) or on axial ^{68}Ga-PSMA HBED-CC PET/CT (E). In conventional CT imaging, only small, unsuspicious LNs could be found (D, arrow). Histopathology revealed overall 9 further LNM in this anatomic field (paraaortic).

around the urinary bladder and the kidneys, potentially obscuring the visibility of tumor lesions and underestimating SUVs (*33,36*). However, when furosemide is used as implemented as routine at our department for PSMA ligand PET imaging, this issue is significantly reduced. Nevertheless, we cannot completely exclude a potential influence on the results of the presented study.

CONCLUSION

This study shows that ^{68}Ga-PSMA HBED-CC PET imaging is a promising method for early detection of LNM in patients with biochemical recurrence of PC after primary treatment. Its efficacy even at low PSA levels and in small-sized LNs is higher than morphologic imaging. Therefore, it could be a promising tool not only for detecting LNM but also for guiding salvage therapy.

DISCLOSURE

The costs of publication of this article were defrayed in part by the payment of page charges. Therefore, and solely to indicate this fact, this article is hereby marked "advertisement" in accordance with 18 USC section 1734. No potential conflict of interest relevant to this article was reported.

REFERENCES

1. Freedland SJ, Presti JC Jr, Amling CL, et al. Time trends in biochemical recurrence after radical prostatectomy: results of the SEARCH database. *Urology.* 2003;61:736–741.
2. Han M, Partin AW, Zahurak M, et al. Biochemical (prostate specific antigen) recurrence probability following radical prostatectomy for clinically localized prostate cancer. *J Urol.* 2003;169:517–523.
3. Chism DB, Hanlon AL, Horwitz EM, et al. A comparison of the single and double factor high-risk models for risk assignment of prostate cancer treated with 3D conformal radiotherapy. *Int J Radiat Oncol Biol Phys.* 2004;59:380–385.
4. Suardi N, Gandaglia G, Gallina A, et al. Long-term outcomes of salvage lymph node dissection for clinically recurrent prostate cancer: results of a single-institution series with a minimum follow-up of 5 years. *Eur Urol.* 2015;67:299–309.
5. Abdollah F, Briganti A, Montorsi F, et al. Contemporary role of salvage lymphadenectomy in patients with recurrence following radical prostatectomy. *Eur Urol.* 2015;67:839–849.
6. Harisinghani MG, Barentsz J, Hahn PF, et al. Noninvasive detection of clinically occult lymph-node metastases in prostate cancer. *N Engl J Med.* 2003;348:2491–2499.
7. Hövels AM, Heesakkers RA, Adang EM, et al. The diagnostic accuracy of CT and MRI in the staging of pelvic lymph nodes in patients with prostate cancer: a meta-analysis. *Clin Radiol.* 2008;63:387–395.
8. Briganti A, Abdollah F, Nini A, et al. Performance characteristics of computed tomography in detecting lymph node metastases in contemporary patients with prostate cancer treated with extended pelvic lymph node dissection. *Eur Urol.* 2012;61:1132–1138.
9. Wibmer AG, Burger IA, Sala E, et al. Molecular imaging of prostate cancer. *Radiographics.* 2016;36:142–159.
10. Scattoni V, Picchio M, Suardi N, et al. Detection of lymph-node metastases with integrated [11C]choline PET/CT in patients with PSA failure after radical retropubic prostatectomy: results confirmed by open pelvic-retroperitoneal lymphadenectomy. *Eur Urol.* 2007;52:423–429.
11. Krause BJ, Souvatzoglou M, Tuncel M, et al. The detection rate of [11C]choline-PET/CT depends on the serum PSA-value in patients with biochemical recurrence of prostate cancer. *Eur J Nucl Med Mol Imaging.* 2008;35:18–23.
12. Fanti S, Minozzi S, Castellucci P, et al. PET/CT with [11C]-choline for evaluation of prostate cancer patients with biochemical recurrence: meta analysis and critical review of available data. *Eur J Nucl Med Mol Imaging.* 2016;43:55–69.
13. Afshar-Oromieh A, Malcher A, Eder M, et al. PET imaging with a [68Ga]gallium-labelled PSMA ligand for the diagnosis of prostate cancer: biodistribution in humans and first evaluation of tumour lesions. *Eur J Nucl Med Mol Imaging.* 2013;40:486–495.
14. Afshar-Oromieh A, Haberkorn U, Hadaschik B, et al. PET/MRI with a ^{68}Ga-PSMA ligand for the detection of prostate cancer. *Eur J Nucl Med Mol Imaging.* 2013;40:1629–1630.
15. Roethke MC, Kuru TH, Afshar-Oromieh A, et al. Hybrid positron emission tomography-magnetic resonance imaging with gallium 68 prostate-specific membrane antigen tracer: a next step for imaging of recurrent prostate cancer—preliminary results. *Eur Urol.* 2013;64:862–864.
16. Afshar-Oromieh A, Zechmann CM, Malcher A, et al. Comparison of PET imaging with a ^{68}Ga-labelled PSMA ligand and ^{18}F-choline-based PET/CT for the diagnosis of recurrent prostate cancer. *Eur J Nucl Med Mol Imaging.* 2014;41:11–20.
17. Afshar-Oromieh A, Avtzi E, Giesel FL, et al. The diagnostic value of PET/CT imaging with the ^{68}Ga-labelled PSMA ligand HBED-CC in the diagnosis of recurrent prostate cancer. *Eur J Nucl Med Mol Imaging.* 2015;42:197–209.
18. Eiber M, Maurer T, Souvatzoglou M, et al. Evaluation of hybrid ^{68}Ga-PSMA ligand PET/CT in 248 patients with biochemical recurrence after radical prostatectomy. *J Nucl Med.* 2015;56:668–674.
19. Maurer T, Gschwend JE, Rauscher I, et al. Diagnostic efficacy of gallium-PSMA positron emission tomography compared to conventional imaging for lymph node staging of 130 consecutive patients with intermediate to high risk prostate cancer. *J Urol.* 2016;195:1436–1443.
20. Eder M, Neels O, Muller M, et al. Novel preclinical and radiopharmaceutical aspects of [68Ga]Ga-PSMA-HBED-CC: a new PET tracer for imaging of prostate cancer. *Pharmaceuticals (Basel).* 2014;7:779–796.
21. Souvatzoglou M, Eiber M, Martinez-Moeller A, et al. PET/MR in prostate cancer: technical aspects and potential diagnostic value. *Eur J Nucl Med Mol Imaging.* 2013;40 suppl 1:S79–S88.
22. Obuchowski NA. Nonparametric analysis of clustered ROC curve data. *Biometrics.* 1997;53:567–578.
23. Smith PJ, Hadgu A. Sensitivity and specificity for correlated observations. *Stat Med.* 1992;11:1503–1509.
24. Genders TS, Spronk S, Stijnen T, et al. Methods for calculating sensitivity and specificity of clustered data: a tutorial. *Radiology.* 2012;265:910–916.
25. Hijazi S, Meller B, Leitsmann C, et al. Pelvic lymph node dissection for nodal oligometastatic prostate cancer detected by ^{68}Ga-PSMA-positron emission tomography/computerized tomography. *Prostate.* 2015;75:1934–1940.
26. Herlemann A, Wenter V, Kretschmer A, et al. Ga-PSMA positron emission tomography/computed tomography provides accurate staging of lymph node regions prior to lymph node dissection in patients with prostate cancer. *Eur Urol.* January 19, 2016 [Epub ahead of print].
27. Rinnab L, Mottaghy FM, Blumstein NM, et al. Evaluation of [11C]-choline positron-emission/computed tomography in patients with increasing prostate-specific antigen levels after primary treatment for prostate cancer. *BJU Int.* 2007;100:786–793.
28. Tilki D, Reich O, Graser A, et al. ^{18}F-fluoroethylcholine PET/CT identifies lymph node metastasis in patients with prostate-specific antigen failure after radical prostatectomy but underestimates its extent. *Eur Urol.* 2013;63:792–796.
29. Maurer T, Weirich G, Schottelius M, et al. Prostate-specific membrane antigen-radioguided surgery for metastatic lymph nodes in prostate cancer. *Eur Urol.* 2015;68:530–534.
30. Freitag MT, Radtke JP, Hadaschik BA, et al. Comparison of hybrid ^{68}Ga-PSMA PET/MRI and ^{68}Ga-PSMA PET/CT in the evaluation of lymph node and bone metastases of prostate cancer. *Eur J Nucl Med Mol Imaging.* 2016;43:70–83.
31. Spick C, Herrmann K, Czernin J. ^{18}F-FDG PET/CT and PET/MRI perform equally well in cancer: evidence from studies on more than 2,300 patients. *J Nucl Med.* 2016;57:420–430.
32. Drzezga A, Souvatzoglou M, Eiber M, et al. First clinical experience with integrated whole-body PET/MR: comparison to PET/CT in patients with oncologic diagnoses. *J Nucl Med.* 2012;53:845–855.
33. Gaertner FC, Beer AJ, Souvatzoglou M, et al. Evaluation of feasibility and image quality of ^{68}Ga-DOTATOC positron emission tomography/magnetic resonance in comparison with positron emission tomography/computed tomography in patients with neuroendocrine tumors. *Invest Radiol.* 2013;48:263–272.
34. Souvatzoglou M, Eiber M, Takei T, et al. Comparison of integrated whole-body [11C]choline PET/MR with PET/CT in patients with prostate cancer. *Eur J Nucl Med Mol Imaging.* 2013;40:1486–1499.
35. Giesel FL, Fiedler H, Stefanova M, et al. PSMA PET/CT with Glu-urea-Lys-(Ahx)-[68Ga(HBED-CC)] versus 3D CT volumetric lymph node assessment in recurrent prostate cancer. *Eur J Nucl Med Mol Imaging.* 2015;42:1794–1800.
36. Afshar-Oromieh A, Haberkorn U, Schlemmer HP, et al. Comparison of PET/CT and PET/MRI hybrid systems using a ^{68}Ga-labelled PSMA ligand for the diagnosis of recurrent prostate cancer: initial experience. *Eur J Nucl Med Mol Imaging.* 2014;41:887–897.

The Journal of NUCLEAR MEDICINE

Value of ^{68}Ga-PSMA HBED-CC PET for the Assessment of Lymph Node Metastases in Prostate Cancer Patients with Biochemical Recurrence: Comparison with Histopathology After Salvage Lymphadenectomy

Isabel Rauscher, Tobias Maurer, Ambros J. Beer, Frank-Philipp Graner, Bernhard Haller, Gregor Weirich, Alan Doherty, Jürgen E. Gschwend, Markus Schwaiger and Matthias Eiber

This article and updated information are available at:
http://jnm.snmjournals.org/content/57/11/1713

Information about reproducing figures, tables, or other portions of this article can be found online at:
http://jnm.snmjournals.org/site/misc/permission.xhtml

Information about subscriptions to JNM can be found at:
http://jnm.snmjournals.org/site/subscriptions/online.xhtml

SNMMI

SOCIETY OF
NUCLEAR MEDICINE
AND MOLECULAR IMAGING